HHS Public Access

Author manuscript

Int J Radiat Oncol Biol Phys. Author manuscript; available in PMC 2024 June 18.

Published in final edited form as:

Int J Radiat Oncol Biol Phys. 2024 April 01; 118(5): 1228–1239. doi:10.1016/j.ijrobp.2023.11.032.

Noninvasive Quantification of Radiation-Induced Lung Injury Using a Targeted Molecular Imaging Probe

Eric Abston, MD, PhD[*], **Iris Y. Zhou, PhD**[†,‡,§], **Jonathan A. Saenger, MD**[‡], **Sergey Shuvaev, PhD**[†,‡,§], **Eman Akam, PhD**[‖], **Shadi A. Esfahani, MD**[‡], **Lida P. Hariri, MD, PhD**[¶], **Nicholas J. Rotile, BS**[†,‡,§], **Elizabeth Crowley, MS**[‡], **Sydney B. Montesi, MD**[#], **Valerie Humblet, PhD**[**], **Grae Arabasz, BS**[†], **Melin Khandekar, MD, PhD**[††], **Ciprian Catana, MD, PhD**[†,§], **Florian J. Fintelmann, MD**[‡], **Peter Caravan, PhD**[†,‡,§], **Michael Lanuti, MD**[*]

[*]Division of Thoracic Surgery, Massachusetts General Hospital, Harvard Medical School, Boston, Massachusetts

[†]Athinoula A. Martinos Center for Biomedical Imaging, Massachusetts General Hospital, Boston, Massachusetts

[‡]Department of Radiology, Massachusetts General Hospital, Harvard Medical School, Boston, Massachusetts

[§]Institute for Innovation in Imaging, Massachusetts General Hospital, Boston, Massachusetts

[‖]Cardiovascular Research Center, Massachusetts General Hospital, Boston, Massachusetts

[¶]Department of Pathology, Massachusetts General Hospital, Harvard Medical School, Boston, Massachusetts

[#]Division of Pulmonary and Critical Care Medicine, Massachusetts General Hospital, Harvard Medical School, Boston, Massachusetts

[**]Collagen Medical LLC, Belmont, Massachusetts

[††]Department of Radiation Oncology, Massachusetts General Hospital, Harvard Medical School, Boston, Massachusetts

Abstract

Purpose: Radiation-induced lung injury (RILI) is a progressive inflammatory process seen after irradiation for lung cancer. The disease can be insidious, often characterized by acute pneumonitis followed by chronic fibrosis with significant associated morbidity. No therapies are approved for RILI, and accurate disease quantification is a major barrier to improved management. Here, we sought to noninvasively quantify RILI using a molecular imaging probe that specifically targets type 1 collagen in mouse models and patients with confirmed RILI.

Corresponding author: Eric Abston, MD, PhD; eabston@mgh.harvard.edu.

Supplementary material associated with this article can be found in the online version at. doi:10.1016/j.ijrobp.2023.11.032.

This protocol is registered with ClinicalTrials.gov and may be viewed online at https://classic.clinicaltrials.gov/ct2/show/NCT04485286ClinicalTrials.gov Identifier: NCT04485286.

Methods and Materials: Using a murine model of lung radiation, mice were imaged with EP-3533, a type 1 collagen probe, to characterize the development of RILI and to assess disease mitigation after losartan treatment. The human analog probe ^{68}Ga-CBP8, targeting type 1 collagen, was tested on excised human lung tissue containing RILI and was quantified via autoradiography. ^{68}Ga-CBP8 positron emission tomography was used to assess RILI in vivo in 6 human subjects.

Results: Murine models demonstrated that probe signal correlated with progressive RILI severity over 6 months. The probe was sensitive to mitigation of RILI by losartan. Excised human lung tissue with RILI had increased binding versus unirradiated control tissue, and ^{68}Ga-CBP8 uptake correlated with collagen proportional area. Human imaging revealed significant ^{68}Ga-CBP8 uptake in areas of RILI and minimal background uptake.

Conclusions: These findings support the ability of a molecular imaging probe targeted at type 1 collagen to detect RILI in preclinical models and human disease, suggesting a role for targeted molecular imaging of collagen in the assessment of RILI.

Introduction

Lung cancer is among the most common cancer types in the world, with 2.2 million new cases annually, and is a leading cause of cancer death.[1] Radiation therapy is a mainstay of treatment for medically inoperable early-stage lung cancers. Radiation-induced lung injury (RILI) is a side effect of radiation therapy marked by radiographic changes outside of the target region observed in up to 70% of patients.[2,3] RILI comprises a spectrum of disease, including asymptomatic radiographic changes, acute pneumonitis, and chronic fibrosis. RILI is often slowly progressive, with the onset of symptoms occurring months after irradiation.[4,5] Although the study of survival in patients with RILI is complicated by coexisting malignancy, RILI appears to negatively affect survival in small studies.[6-8]

There are currently no reliable methods to diagnose RILI, predict disease course, or measure treatment effects. RILI remains a diagnosis of exclusion in patients with a history of radiation exposure after other causes of lung disease, such as recurrent malignancy and infection, have been ruled out. Common grading systems used to quantify RILI rely heavily on individual patient symptoms and lack objective standards.[9-11] High-resolution computed tomography is the most common modality used in the clinical evaluation of RILI, but changes in attenuation do not always indicate the presence of disease. ^{18}F-Fluorodeoxyglucose positron emission tomography (PET), magnetic resonance imaging (MRI), and single-photon emission computed tomography have also been used experimentally with some success[12-15] but are not part of RILI diagnosis or management at this time.

Clinical management of RILI has proven difficult, and there is currently no Food and Drug Administration–approved treatment for RILI. Steroids are empirically given to treat pneumonitis, and early studies suggest some benefit with pentoxyfiline and angiotensin-converting enzyme inhibitors in humans and animals.[16-18] A recent trial evaluating nintedanib in RILI failed to show benefit.[19] The most successful strategies for RILI have come with advances in limiting the radiation dose and volume of irradiated lung as well as

through careful risk stratification of patients with known factors, including age, concomitant pulmonary fibrosis, and chemotherapy.[5]

Molecular imaging probes targeted at type 1 collagen for detecting and staging tissue fibrosis have recently been developed. These probes are based on a 16–amino acid cyclic peptide derived from a phage display screen. An MRI probe, termed EP-3533, had 3 gadolinium chelates conjugated to the peptide,[20,21] while a PET probe (^{68}Ga-CBP8) conjugated the positron emitting isotope gallium 68 for detection. EP-3533-enhanced MRI can quantify pulmonary fibrosis in the mouse bleomycin injury model[22] and in rodent models of cardiac, renal, and liver fibrosis.[20,22-26] ^{68}Ga-CBP8 PET was shown to be specific for pulmonary fibrosis in mouse models and explanted human lung tissue and that PET signal increased with lung collagen content.[27] In humans, ^{68}Ga-CBP8 is well tolerated and shows rapid clearance via the kidneys with low signal in healthy lungs.[28] Patients with idiopathic pulmonary fibrosis showed significantly higher lung uptake of ^{68}Ga-CBP8.

In this study, we test the hypothesis that fibrosis due to RILI can be identified by type 1 collagen molecular imaging. We developed a murine model of RILI and tested the ability of EP-3533-enhanced MRI to quantify pulmonary fibrosis in RILI over a time course of disease progression and mitigation treatment with losartan (Los). This common blood pressure medication has known antifibrotic activity and has been successfully tested in radiation exposure mitigation models.[29] To further translate this work, we assayed the specific binding of ^{68}Ga-CBP8 to explanted human RILI lung tissue. Finally, we tested the ability of ^{68}Ga-CBP8 PET to detect RILI in vivo in individuals with established RILI.

Methods and Materials

Mouse models

Animal studies were approved by the Institutional Animal Care and Use Committee at the Massachusetts General Hospital. RILI models are described in Appendix E1. Briefly, male 12-week-old C57L/J mice received 16-Gy delivered dose (exposure dose of 21 Gy) to the right hemithorax and underwent imaging 3 months (3M) or 6 months (6M) post-exposure. A subset of mice received Los (40 mg/kg/d) in drinking water. Los treatment via drinking water was initiated immediately after irradiation and was maintained continuously until animal euthanasia. Lung imaging was performed as previously described[20] using EP-3533, and tissue was collected for analysis as described in Appendix E1.

Human studies

Human studies were approved by the institutional review board at the Massachusetts General Hospital under the approval of the U.S. Food and Drug Administration and are registered at ClinicalTrials.gov. Ex vivo studies were performed on tissue collected from individuals with either RILI or healthy lungs. Probe detection of RILI was performed via autoradiography.[27]

In vivo studies

The following were the inclusion criteria used: age 18 to 80 years, stage I to III non-small cell lung carcinoma, received radiation therapy as routine care for lung cancer, and was

diagnosed with radiographically apparent RILI by a treating physician. The following were the exclusion criteria used: estimated glomerular filtration rate <30, stage IV cancer, pregnant or breastfeeding, body mass index >33, known history of pulmonary disease, active smoker, had a pulmonary infection in the past 6 weeks, and contraindication to MRI. After consent and physical examination, participants received intravenous ^{68}Ga-CBP8 at a dose of approximately 173 MBq (range, 148-236 MBq). Two radiologists independently reviewed the acquired MR/PET data and compared it with recent clinical computed tomography scans to identify a region of interest (ROI) corresponding to RILI in each participant, and a contralateral ROI of similar size was identified with normal-appearing lung. PET signal from 40 to 75 minutes after probe injection was quantified in the ROIs containing both RILI and normal lung. Additional descriptions are provided in Appendix E1.

Statistical analysis

All statistical analyses were performed using GraphPad (Prism version 6). Differences between groups were determined by using a 1-way analysis of variance (ANOVA) with a post hoc Bonferroni correction. Pearson correlation was used for the analysis of linear correlation of data.

Results

Type 1 collagen probe sensitivity to progression of RILI

We first sought to establish a murine model of RILI, which accurately reproduced its characteristic progressive fibrotic changes, and test whether a type 1 collagen probe could noninvasively measure time-dependent changes in disease severity. After a single exposure of 16 Gy to the right hemithorax, mice underwent imaging at either 3M or 6M time points, and probe uptake was compared with that of unirradiated controls (0 Gy; Fig. 1A).

The lungs of irradiated mice demonstrated significant markers of RILI, which were progressive over time. Hematoxylin and eosin (H&E) stain and Masson's trichrome stain demonstrated cellular infiltrate, alveolar thickening, consolidation, and collagen deposition consistent with prior descriptions of RILI,[4,30] which progressed from 3M to 6M with additional fibrosis and alveolar consolidation (Fig. 1B). Collagen proportional area (CPA) was significantly increased in mice at both 3M and 6M time points compared with nonirradiated controls (ANOVA $P < .001$; post hoc: 0M 16 ± 0.2% vs 3M 29 ± 0.7%, $P < .001$; 0M vs 6M 36 ± 1.9%, $P < .001$; 3M vs 6M $P = .03$; Fig. 2E). Additionally, Ashcroft scores were significantly elevated in the irradiated groups (ANOVA $P < .001$; post hoc: 0M 0.06 ± 0.01 vs 3M 2.50 ± 0.15; $P < .001$; 0M vs 6M 3.1 ± 0.14, $P < .001$; 3M vs 6M $P < .001$; Fig. 2F). Hydroxyproline, a measure of collagen deposition in RILI, was also significantly elevated with irradiation (ANOVA $P < .001$; post hoc: 0M 130 ± 7 μg/lung vs 3M 201 ± 10 μg/lung, $P < .001$; 0M vs 6M 260 ± 7 μg/lung $P < .001$; 3M vs 6M $P = .003$; Fig. 2D).

Representative ultrashort echo time (UTE) T1-weighted axial MR images acquired before and 40 minutes after EP-3533 administration and UTE subtraction images (40 minutes

postinjection – preinjection) demonstrated increases in right lung signal enhanced by EP-3533 (Fig. 1C).

Figure 1D demonstrates colocalization of lung injury in the irradiated right hemithorax. Masson's trichrome stain shows diffuse injury throughout the right lung but not in the left lung. The T1-weighted coronal MR image shows ground glass opacities in the right hemithorax and normal-appearing lung on the left. The subtraction image illustrates substantial signal enhancement in the right lung, whereas little enhancement is observed in the uninjured left lung.

The change in contrast-to-noise ratio (ΔCNR) versus time after EP-3533 injection for 0M, 3M, and 6M postirradiation groups are shown in Figure 2A. The area under the curve (AUC) for ΔCNR versus time was elevated in the irradiated groups (ANOVA, $P < .001$; post hoc: 0M 60 ± 6 ΔCNR × minutes vs 3M 172 ± 14 ΔCNR × minutes, $P < .001$; 0M vs 6M 316 ± 20 μCNR × minutes, $P < .001$; 3M vs 6M $P < .001$; Fig. 2B). The ΔCNR at 40 minutes postcontrast injection has previously been identified as having the largest signal-to-noise ratio in fibrotic tissue[25] and was elevated after irradiation (ANOVA, $P < .001$; post hoc: 0M 1.4 ± 0.2 vs 3M 4.2 ± 0.4, $P < .001$; 0M vs 6M 7.9 ± 0.6, $P < .001$; Fig. 2C).

To test the strength of the association between markers of RILI severity and EP-3533 signal, disease severity data (CPA, Ashcroft score, and hydroxyproline) from each time point were plotted against the corresponding ΔCNR value at 40 minutes postinjection for that animal. Significant correlations were found for each metric (hydroxyproline vs ΔCNR: $r = 0.94$, $P < .001$ [Fig. 2G]; CPA vs ΔCNR: $r = 0.95$, $P < .001$ [Fig. 2H]; Ashcroft score vs ΔCNR: $r = 0.90$, $P < .001$ [Fig. 2I]).

Effects of Los on mitigation of RILI

We next sought to test probe sensitivity to detect disease modification. Los is an angiotensin receptor blocker with well-known antifibrotic properties, which has been previously shown to improve RILI in both rodent models and in preliminary human studies.[16,18,31-34] At 3M postexposure, mice underwent imaging before tissue collection (Fig. 3A). A visual comparison of the untreated radiation treatment (XRT) and Los-treated XRT groups via H&E- and Masson's trichrome–stained sections revealed fewer cellular infiltrates, diminished collagen deposition, and less alveolar thickening in the Los-treated group (Fig. 3B). Representative MR images demonstrate increased probe signal following irradiation, which was diminished with Los treatment.

Irradiation followed by Los treatment mitigated RILI but did not eliminate it completely. CPA was elevated in the 16 Gy + Los group compared with the 0 Gy + Los group but was significantly lower than in the 16 Gy + vehicle (Veh) group (ANOVA $P < .001$; post hoc: 0 Gy + Los 17 ± 0.6% vs 16 Gy + Los 23 ± 1%, $P = .005$; 16 Gy + Veh 29 ± 0.7% vs 16 Gy + Los, $P = .009$; Fig. 4E). The Ashcroft score was similarly improved with Los (ANOVA $P < .001$; post hoc: 0 Gy + Los 0.2 ± 0.01 vs 16 Gy + Los 1.1 ± 0.06, $P = .018$; 16 Gy + Veh 2.5 ± 0.15 vs 16 Gy + Los, $P = .005$; Fig. 4F). Hydroxyproline confirmed this trend (ANOVA $P < .001$; post hoc: 0 Gy + Los 143 ± 6 μg/lung vs 16 Gy + Los 169 ± 5 μg/lung, $P = .022$; 16 Gy + Veh 201 ± 10 μg/lung vs 16 Gy + Los, $P < .001$; Fig. 4D).

Time-dependent EP-3533 ΔCNR is displayed in Figure 4A. The AUC analysis (Fig. 4B) resolved the increase in signal from irradiation and detected the treatment effect of Los (ANOVA $P < .001$; post hoc: 0 Gy + Los 41 ± 8 ΔCNR × minutes vs 16 Gy + Los 91 ± 7 ΔCNR × minutes, $P < .001$; 16 Gy + Veh 172 ± 14 ΔCNR × minutes vs 16 Gy + Los, $P < .001$). Similarly, ΔCNR at 40 minutes postinjection confirmed this result (ANOVA $P < .001$; post hoc: 0 Gy + Los 1 ± 0.2 vs 16 Gy + Los 2 ± 0.2, $P < .001$; 16 Gy + Veh 4.2 ± 0.4 vs 16 Gy + Los, $P < .001$; Fig. 4C).

Significant correlations between the MRI metric ΔCNR at 40 minutes postinjection and biochemical and histologic measures of fibrosis were found for each metric (hydroxyproline vs ΔCNR: $r = 0.85$, $P < .001$ [Fig. 4G]; CPA vs ΔCNR: $r = 0.84$, $P < .001$ [Fig. 4H]; Ashcroft score vs ΔCNR: $r = 0.89$, $P < .001$ [Fig. 4I]). These results confirm a strong correlation between markers of RILI severity and collagen probe signal in the detection of a pharmacologic mitigation effect.

Collagen probe detection of RILI in explanted human tissue

Human lung tissues in individuals with RILI (n = 3) and unirradiated subjects (n = 3) were collected and characterized (Table E1). H&E and Masson's trichrome stains show alveolar thickening, cellular infiltration, and collagen deposition in irradiated lung tissue (Fig. 5A). Analysis via CPA showed a significant increase in irradiated tissue (XRT 39 ± 2 vs control 28 ± 2%, $P = .015$). Hydroxyproline was also significantly elevated in irradiated tissue (control 3150 ± 249 vs XRT 4116 ± 185 μg/g, $P = .036$). Signal from human lung tissue sections incubated with ^{68}Ga-CBP8 was significantly increased in RILI tissue (XRT 11,807 ± 789 vs control 8584 ± 95 digital light units, $P = .015$). The ^{68}Ga-CBP8 signal was normalized to the signal from a nonbinding linear peptide control probe, ^{68}Ga-Ctrl, to further assess specificity. The ratio of ^{68}Ga-CBP8 to ^{68}Ga-Ctrl autoradiography signal was significantly higher in RILI tissue (control 1.8 ± 0.1 vs XRT 2.9 ± 0.3, $P = .021$; Fig. 5C). Representative images of probe uptake are shown in Figure 5B.

The strength of the relationship between ^{68}Ga-CBP8 and each RILI severity metric was assessed. A significant correlation was found for CPA (CPA vs fold change: $r = 0.87$, $P = .026$; Fig. 5D), but hydroxyproline was not significantly associated with fold change (hydroxyproline vs fold change: $r = 0.67$, $P > .05$; Fig. 5E).

In vivo imaging of RILI in humans with ^{68}Ga-CBP8

We evaluated RILI in 6 individuals who underwent radiation therapy as part of routine treatment for lung cancer (Table E2). Computed tomography images of the irradiated lung confirm RILI (Fig. 6). Fused PET-MR images demonstrate increased ^{68}Ga-CBP8 uptake in the area of RILI. Subject 1 received ^{68}Ga-CBP8 while in the scanner, and the probe's dynamic washout curve was measured (Fig. E2). No participants in the study had recurrence in the defined ROI where probe signal was measured, with a minimum follow-up period of 18 months.

The mean standardized uptake values (SUVs) 40 to 75 minutes postinjection were computed and compared with areas of contralateral healthy lung. Mean SUV in areas of RILI (1.23 ± 0.19) was significantly increased over that of healthy lung (0.35 ± 0.04, $P < .001$).

The 35-minute PET acquisition was binned into 5-minute frames. SUV_{mean} values for RILI, healthy lung, and blood pool ROIs were quantified to produce washout curves (Fig. 6B). The tissue-to-blood ratio was calculated for both RILI and healthy lung ROIs graphed against time after injection (Fig. 6C). This graph produces a flat curve and suggests that the probe is stable at this point in its washout curve and is appropriate for analyzing the probe signal. The mean $SUV\text{-}_{mean}$ signal from 40 to 75 minutes postinjection for the RILI ROI was significantly higher than the healthy lung ROI (1.2 ± 0.2 vs 0.4 ± 0.1, $P = .005$; Fig. 6D). The tissue-to-blood ratio for RILI was also significantly increased compared with the healthy lung ROI (0.64 ± 0.06 vs 0.19 ± 0.02, $P < .0001$; Fig. 6E). These results indicate a greater affinity of ^{68}Ga-CBP8 for areas of RILI than for healthy lung.

Discussion

We demonstrated in a preclinical model of RILI that noninvasive molecular imaging techniques using a probe specific to type 1 collagen are sensitive to changes in RILI, both with the natural progression of disease over time and with pharmacologic disease modification. Type 1 collagen molecular MR imaging with EP-3533 was highly correlated with established markers of RILI, such as hydroxyproline and histologic analysis. Because this MR probe is not available for human use, we used an analogous PET probe, ^{68}Ga-CBP8, that used the same collagen-targeting peptide and that was available for human studies. We tested the binding and specificity of ^{68}Ga-CBP8 to RILI in human tissue using autoradiography and showed that the collagen probe signal was again highly correlated with RILI severity. Finally, we demonstrated the ability of ^{68}Ga-CBP8 to detect RILI in humans in vivo. This approach to molecular detection of collagen deposition in irradiated lungs is novel and has not been described in humans.

In humans and animals, RILI is slowly progressive with early pneumonitis and chronic fibrosis stages[30,35] and shares common signaling pathways with other fibrotic lung diseases.[36] As RILI models are slow moving and mimic human disease, they may be ideal for the study of novel therapeutics for fibrotic lung disease. Murine models of pulmonary fibrosis and fibrogenesis are a commonly used preclinical model for the development of molecular imaging probes.[37] Previously, probes targeted to type 1 collagen were tested in a bleomycin model as well as another probe directed at a key step in collagen synthesis.[27,38-40] However, this is the first attempt to explore molecular imaging techniques in preclinical RILI models.

Inhibition of the renin-angiotensin pathway has been studied as a mitigation agent in preclinical models of RILI[18,31] and has been associated with improved radiation-induced pneumonitis in humans. In 2 small retrospective studies, angiotensin-converting enzyme inhibitor use was associated with reduced rates of symptomatic radiation pneumonitis from a baseline of 16% to 4% in one study and from 11% to 2% in the other.[16,32] Another retrospective study showed less symptomatic radiation-induced pneumonitis in a subgroup analysis of male participants and low-dose radiation.[34] A prospective trial was attempted but closed early due to low subject accrual.[33] These studies illustrate the need for more sophisticated methods to evaluate RILI.

In humans, molecular imaging techniques have been successfully applied to idiopathic pulmonary fibrosis, with molecular probes directed at various aspects of fibrosis, including type 1 collagen,[28] chemokine receptor 2,[41] $\alpha_V\beta_6$ integrin,[42] cathepsin protease,[43] and glycolytic metabolism.[44] However, molecular imaging studies have yet to focus on RILI. Significant work has been done to quantify RILI using more traditional techniques.[45] The study of RILI via noninvasive molecular imaging techniques represents a unique opportunity, as the timing, location, and dose are carefully recorded, and the patients are carefully followed thereafter. Noninvasive quantification of RILI offers the possibility of using molecules specific to the disease process, such as type 1 collagen, to resolve subtle changes in disease with therapeutics that are undetectable with current methods.

This technology shows great promise as a diagnostic tool capable of detecting subtle changes in RILI progression that adds to information currently obtained by computed tomography. Imaging enhanced with ^{68}Ga-CBP8 could allow us to detect subtle changes in RILI progression and provide important prognostic information for the development of RILI and other fibrotic diseases. Although the blood SUV measured from the pulmonary artery reflects the nonspecific background signal, its contribution toward tissue SUV is limited by the fractional volume of blood in the lung parenchyma. Further correction of such nonspecific background requires accurate mapping of the blood volume fraction, which is currently under investigation. Nevertheless, despite relatively high blood SUV over time, the contrast between RILI and normal lung remains more than 3-fold (Fig. 6C), offering great sensitivity in detecting RILI. Although not yet tested in humans, the probe is capable of detecting treatment-induced changes in RILI in mice. This technique could provide a highly sensitive assay for drug trials, an unmet need that will be essential to develop therapeutics for RILI. By resolving subtle changes in early disease, this technique could help identify individuals at high risk for severe RILI before they develop symptoms. Finally, this technology could be used to assist in determining whether an opacity seen on computed tomography is due to cancer recurrence, infection, or RILI. In mice, this technology offers the exciting possibility of noninvasively assessing disease burden at multiple time points throughout an experiment.

The findings of this study need to be interpreted in light of its small sample size. More work is required to fully correlate ^{68}Ga-CBP8 signal with specific histopathologic findings and to develop the association between hydroxyproline and ^{68}Ga-CBP8 into a robust quantitative method. Individuals were imaged using MR/PET, which makes comparison of our findings with clinical computed tomography scans via coregistration difficult. The chemotherapy that was used for the 3 nonirradiated individuals in Figure 5 included a platinum-based modality (cisplatin or carboplatin) in combination with pemetrexed or etoposide, whereas only 1 of the 3 individuals in the irradiated group received this therapy–a potential confounding factor. However, these chemotherapies are historically associated with a low probability of pulmonary toxicity or fibrosis and are unlikely to have significantly affected the response to radiation therapy. Furthermore, the clinical computed tomography chest scans that were part of the standard of oncologic care for these individuals did not show appreciable pulmonary toxicity outside the radiation field during surveillance imaging after chemotherapy. Further studies on probe uptake after radiation and correlation to clinical symptoms are needed to develop ^{68}Ga-CBP8 as a biomarker of clinically significant RILI.

Conclusion

The noninvasive monitoring of type 1 collagen via molecular imaging techniques in both clinical and preclinical RILI will enhance our assessment of the disease. This technique offers new opportunities to noninvasively monitor RILI, with potential applications in both disease prognosis and assessment of treatment response. This study is the first step in expanding techniques that have been focused on traditional pulmonary fibrosis in the study of RILI.

Supplementary Material

Refer to Web version on PubMed Central for supplementary material.

Acknowledgments—

We thank Dr John Moulder of the Medical College of Wisconsin for his advice regarding radiation injury models and Dr Alexsia Richards of the Whitehead Institute for her assistance with figures.

Disclosures:

V.H. and P.C. own interest in Collagen Medical, LLC, the entity holding intellectual property rights to molecular probes used in this article. This work was funded by a CHEST Foundation Research Grant in Pulmonary Fibrosis (K08CA259626, K23HL150331, R01HL153606, and 4R44CA250771-02, 2019).

Data Sharing Statement:

Research data are not available at this time.

References

1. Sung H, Ferlay J, Siegel RL, et al. Global Cancer Statistics 2020: GLOBOCAN estimates of incidence and mortality worldwide for 36 cancers in 185 countries. CA Cancer J Clin 2021;71:209–249. [PubMed: 33538338]
2. Li Y, Dykstra M, Best TD, et al. Differential inflammatory response dynamics in normal lung following stereotactic body radiation therapy with protons versus photons. Radiother Oncol 2019;136:169–175. [PubMed: 31015121]
3. Takeda A, Kunieda E, Takeda T, et al. Possible misinterpretation of demarcated solid patterns of radiation fibrosis on CT scans as tumor recurrence in patients receiving hypofractionated stereotactic radiotherapy for lung cancer. Int J Radiat Oncol Biol Phys 2008;70:1057–1065. [PubMed: 17905527]
4. Rahi MS, Parekh J, Pednekar P, et al. Radiation-induced lung injury—current perspectives and management. Clin Pract 2021;11:410–429. [PubMed: 34287252]
5. Marks LB, Yu X, Vujaskovic Z, Small W Jr, Folz R, Anscher MS. Radiation-induced lung injury. Semin Radiat Oncol 2003;13:333–345. [PubMed: 12903021]
6. Butof R, Kirchner K, Appold S, et al. Potential clinical predictors of outcome after postoperative radiotherapy of non-small cell lung cancer. Strahlenther Onkol 2014;190:263–269. [PubMed: 24413893]
7. Inoue A, Kunitoh H, Sekine I, Sumi M, Tokuuye K, Saijo N. Radiation pneumonitis in lung cancer patients: A retrospective study of risk factors and the long-term prognosis. Int J Radiat Oncol Biol Phys 2001;49:649–655. [PubMed: 11172945]
8. Wang JY, Chen KY, Wang JT, et al. Outcome and prognostic factors for patients with non-small-cell lung cancer and severe radiation pneumonitis. Int J Radiat Oncol Biol Phys 2002;54:735–741. [PubMed: 12377325]

9. Cox JD, Stetz J, Pajak TF. Toxicity criteria of the Radiation Therapy Oncology Group (RTOG) and the European Organization for Research and Treatment of Cancer (EORTC). Int J Radiat Oncol Biol Phys 1995;31:1341–1346. [PubMed: 7713792]
10. Trotti A, Colevas AD, Setser A, et al. CTCAE v3.0: Development of a comprehensive grading system for the adverse effects of cancer treatment. Semin Radiat Oncol 2003;13:176–181. [PubMed: 12903007]
11. Dueck AC, Mendoza TR, Mitchell SA, National Cancer Institute PROCSG. Validity and reliability of the US National Cancer Institute's Patient-Reported Outcomes version of the Common Terminology Criteria for Adverse Events (PRO-CTCAE). JAMA Oncol 2015;1:1051–1059. [PubMed: 26270597]
12. Mah K, Van Dyk J. Quantitative measurement of changes in human lung density following irradiation. Radiother Oncol 1988;11:169–179. [PubMed: 3353521]
13. Marks LB, Spencer DP, Bentel GC, et al. The utility of SPECT lung perfusion scans in minimizing and assessing the physiologic consequences of thoracic irradiation. Int J Radiat Oncol Biol Phys 1993;26:659–668. [PubMed: 8330998]
14. Guerrero T, Johnson V, Hart J, et al. Radiation pneumonitis: Local dose versus [^{18}F]-fluorodeoxyglucose uptake response in irradiated lung. Int J Radiat Oncol Biol Phys 2007;68:1030–1035. [PubMed: 17398033]
15. Fain S, Schiebler ML, McCormack DG, Parraga G. Imaging of lung function using hyperpolarized helium-3 magnetic resonance imaging: Review of current and emerging translational methods and applications. J Magn Reson Imaging 2010;32:1398–1408. [PubMed: 21105144]
16. Kharofa J, Cohen EP, Tomic R, Xiang Q, Gore E. Decreased risk of radiation pneumonitis with incidental concurrent use of angiotensin-converting enzyme inhibitors and thoracic radiation therapy. Int J Radiat Oncol Biol Phys 2012;84:238–243. [PubMed: 22300564]
17. Ozturk B, Egehan I, Atavci S, Kitapci M. Pentoxifylline in prevention of radiation-induced lung toxicity in patients with breast and lung cancer: A double-blind randomized trial. Int J Radiat Oncol Biol Phys 2004;58:213–219. [PubMed: 14697441]
18. Medhora M, Gao F, Jacobs ER, Moulder JE. Radiation damage to the lung: Mitigation by angiotensin-converting enzyme (ACE) inhibitors. Respirology 2012;17:66–71. [PubMed: 22023053]
19. Rimner A, Moore ZR, Lobaugh S, et al. Randomized, phase II, placebo-controlled trial of nintedanib for the treatment of radiation pneumonitis. Int J Radiat Oncol Biol Phys 2023;116:1091–1099. [PubMed: 36889516]
20. Caravan P, Das B, Dumas S, et al. Collagen-targeted MRI contrast agent for molecular imaging of fibrosis. Angew Chem Int Ed Engl 2007;46:8171–8173. [PubMed: 17893943]
21. Kolodziej AF, Zhang Z, Overoye-Chan K, Jacques V, Caravan P. Peptide optimization and conjugation strategies in the development of molecularly targeted magnetic resonance imaging contrast agents. Methods Mol Biol 2014;1088:185–211. [PubMed: 24146405]
22. Caravan P, Yang Y, Zachariah R, et al. Molecular magnetic resonance imaging of pulmonary fibrosis in mice. Am J Respir Cell Mol Biol 2013;49:1120–1126. [PubMed: 23927643]
23. Fuchs BC, Wang H, Yang Y, et al. Molecular MRI of collagen to diagnose and stage liver fibrosis. J Hepatol 2013;59:992–998. [PubMed: 23838178]
24. Li S, Ghoshal S, Sojoodi M, et al. The farnesoid X receptor agonist EDP-305 reduces interstitial renal fibrosis in a mouse model of unilateral ureteral obstruction. FASEB J 2019;33:7103–7112. [PubMed: 30884252]
25. Helm PA, Caravan P, French BA, et al. Postinfarction myocardial scarring in mice: Molecular MR imaging with use of a collagen-targeting contrast agent. Radiology 2008;247:788–796. [PubMed: 18403626]
26. Zhou IY, Clavijo Jordan V, Rotile NJ, et al. Advanced MRI of liver fibrosis and treatment response in a rat model of nonalcoholic steato- hepatitis. Radiology 2020;296:67–75. [PubMed: 32343209]
27. Desogere P, Tapias LF, Hariri LP, et al. Type I collagen-targeted PET probe for pulmonary fibrosis detection and staging in preclinical models. Sci Transl Med 2017;9:eaaf4696. [PubMed: 28381537]

28. Montesi SB, Izquierdo-Garcia D, Desogere P, et al. Type I collagen-targeted positron emission tomography imaging in idiopathic pulmonary fibrosis: First-in-human studies. Am J Respir Crit Care Med 2019;200:258–261. [PubMed: 31161770]
29. Moulder JE, Cohen EP, Fish BL. Captopril and losartan for mitigation of renal injury caused by single-dose total-body irradiation. Radiat Res 2011;175:29–36. [PubMed: 21175344]
30. Down JD, Nicholas D, Steel GG. Lung damage after hemithoracic irradiation: Dependence on mouse strain. Radiother Oncol 1986;6:43–50. [PubMed: 3715060]
31. Medhora M, Gao F, Wu Q, et al. Model development and use of ACE inhibitors for preclinical mitigation of radiation-induced injury to multiple organs. Radiat Res 2014;182:545–555. [PubMed: 25361399]
32. Alite F, Balasubramanian N, Adams W, Surucu M, Mescioglu I, Harkenrider MM. Decreased risk of radiation pneumonitis with coincident concurrent use of angiotensin-converting enzyme inhibitors in patients receiving lung stereotactic body radiation therapy. Am J Clin Oncol 2018;41:576–580. [PubMed: 27560156]
33. Small W Jr, James JL, Moore TD, et al. Utility of the ACE inhibitor cap- topril in mitigating radiation-associated pulmonary toxicity in lung cancer: Results from NRG Oncology RTOG 0123. Am J Clin Oncol 2018;41:396–401. [PubMed: 27100959]
34. Wang H, Liao Z, Zhuang Y, et al. Do angiotensin-converting enzyme inhibitors reduce the risk of symptomatic radiation pneumonitis in patients with non-small cell lung cancer after definitive radiation therapy? Analysis of a single-institution database. Int J Radiat Oncol Biol Phys 2013;87:1071–1077. [PubMed: 24161424]
35. Beach TA, Groves AM, Williams JP, Finkelstein JN. Modeling radiation-induced lung injury: Lessons learned from whole thorax irradiation. Int J Radiat Biol 2020;96:129–144. [PubMed: 30359147]
36. Rubin P, Johnston CJ, Williams JP, McDonald S, Finkelstein JN. A perpetual cascade of cytokines postirradiation leads to pulmonary fibrosis. Int J Radiat Oncol Biol Phys 1995;33:99–109. [PubMed: 7642437]
37. Desogere P, Montesi SB, Caravan P. Molecular Probes for Imaging Fibrosis and Fibrogenesis. Chemistry 2018;25:1128–1141. [PubMed: 30014529]
38. Desogere P, Tapias LF, Rietz TA, et al. Optimization of a collagen-targeted PET probe for molecular imaging of pulmonary fibrosis. J Nucl Med 2017;58:1991–1996. [PubMed: 28611243]
39. Akam EA, Abston E, Rotile NJ, et al. Improving the reactivity of hydrazine-bearing MRI probes for in vivo imaging of lung fibrogenesis. Chem Sci 2020;11:224–231. [PubMed: 32728411]
40. Wahsner J, Desogere P, Abston E, et al. ^{68}Ga-NODAGA-indole: An allysine-reactive positron emission tomography probe for molecular imaging of pulmonary fibrogenesis. J Am Chem Soc 2019;141:5593–5596. [PubMed: 30908032]
41. Brody SL, Gunsten SP, Luehmann HP, et al. Chemokine receptor 2-targeted molecular imaging in pulmonary fibrosis. A clinical trial. Am J Respir Crit Care Med 2021;203:78–89. [PubMed: 32673071]
42. Lukey PT, Coello C, Gunn R, et al. Clinical quantification of the integrin $\alpha_v\beta_6$ by [^{18}F]FB-A20FMDV2 positron emission tomography in healthy and fibrotic human lung (PETAL Study). Eur J Nucl Med Mol Imaging 2020;47:967–979. [PubMed: 31814068]
43. Withana NP, Ma X, McGuire HM, et al. Non-invasive imaging of idiopathic pulmonary fibrosis using cathepsin protease probes. Sci Rep 2016;6:19755. [PubMed: 26797565]
44. Lukey PT, Harrison SA, Yang S, et al. A randomised, placebo-controlled study of omipalisib (PI3K/mTOR) in idiopathic pulmonary fibrosis. Eur Respir J 2019;53:1801992. [PubMed: 30765508]
45. Robbins ME, Brunso-Bechtold JK, Peiffer AM, Tsien CI, Bailey JE, Marks LB. Imaging radiation-induced normal tissue injury. Radiat Res 2012;177:449–466. [PubMed: 22348250]

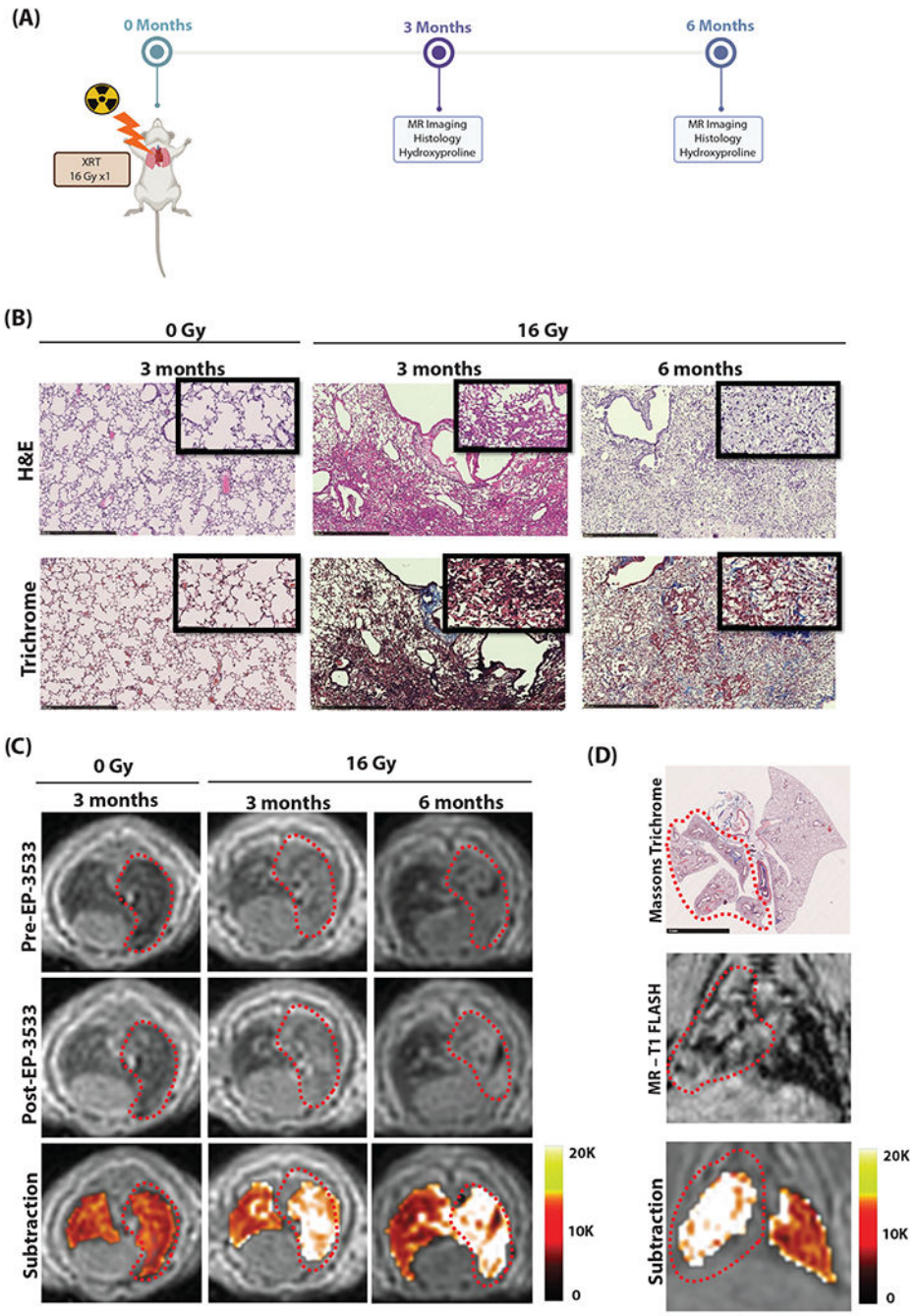

Fig. 1.

(A) Murine model of progressive radiation-induced lung injury. Mice underwent a single dose of 16 Gy to the right hemithorax and were imaged at either 3 or 6 months after irradiation. (B) Representative hematoxylin and eosin (H&E; top) and trichrome (bottom) stains of the right lung show normal lung architecture in unirradiated (0 Gy) mice. Mice at 3 months developed cellular infiltrate, alveolar thickening, consolidation, and collagen deposition. By 6 months, significant fibrosis and alveolar consolidation was seen. (C) Representative axial magnetic resonance (MR) images are shown before and after EP-3533

injection. Lungs of unirradiated mice (0 Gy) show low signal on ultrashort echo time MR. Irradiated mice show increasing right lung signal from 3 to 6 months due to consolidation, and these areas are enhanced after EP-3533 administration. False color subtraction images (40 minutes after EP-3533 injection — preinjection) overlaid on preinjection ultrashort echo time images demonstrate increased signal enhancement in irradiated lung. (D) Colocalization of lung injury in the irradiated right hemithorax on pathology and coronal MR images. Diffuse injury throughout the right lung but not in the left lung is seen on Masson's trichrome and MR-T1FLASH images. The false color subtraction image illustrates substantial signal enhancement in the right lung but not in the nonirradiated left lung.
Abbreviation: XRT = Radiation treatment.

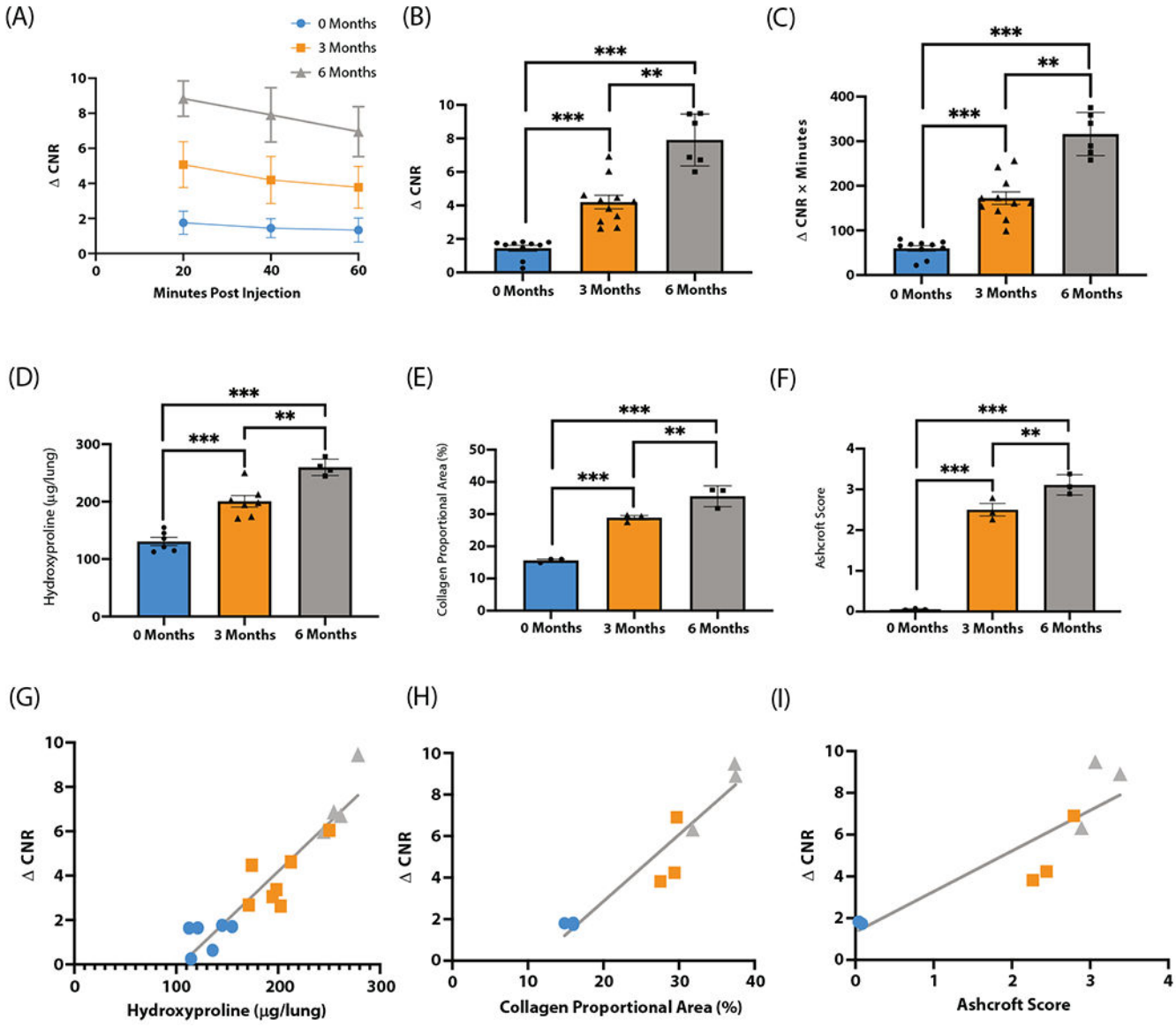

Fig. 2.

EP-3533 detects progressive radiation-induced lung injury (RILI) in a murine model. (A) Change in contrast-to-noise ratio (ΔCNR) versus time curves show progressively increased EP-3533-enhanced magnetic resonance signal at 3 months and 6 months after irradiation. (B) ΔCNR at 40 minutes postinjection is progressively elevated from 0 months, 3 months, and 6 months after irradiation. (C) Area under the curve quantification also demonstrated similar elevations in EP-3533 signal. (D-F) Validated techniques used to quantify RILI include hydroxyproline (D), collagen proportional area (E), and Ashcroft score (F). Each technique demonstrates increasing severity of RILI over time postirradiation with analysis of variance and Bonferroni post hoc *t* test. (G-I) Associations between EP-3533 and hydroxyproline (G), collagen proportional area (H), and Ashcroft score (I) were assessed via Pearson correlation, and EP-3533 was significantly correlated with RILI severity in each (*$P < .05$, **$P < .001$, ***$P < .0001$).

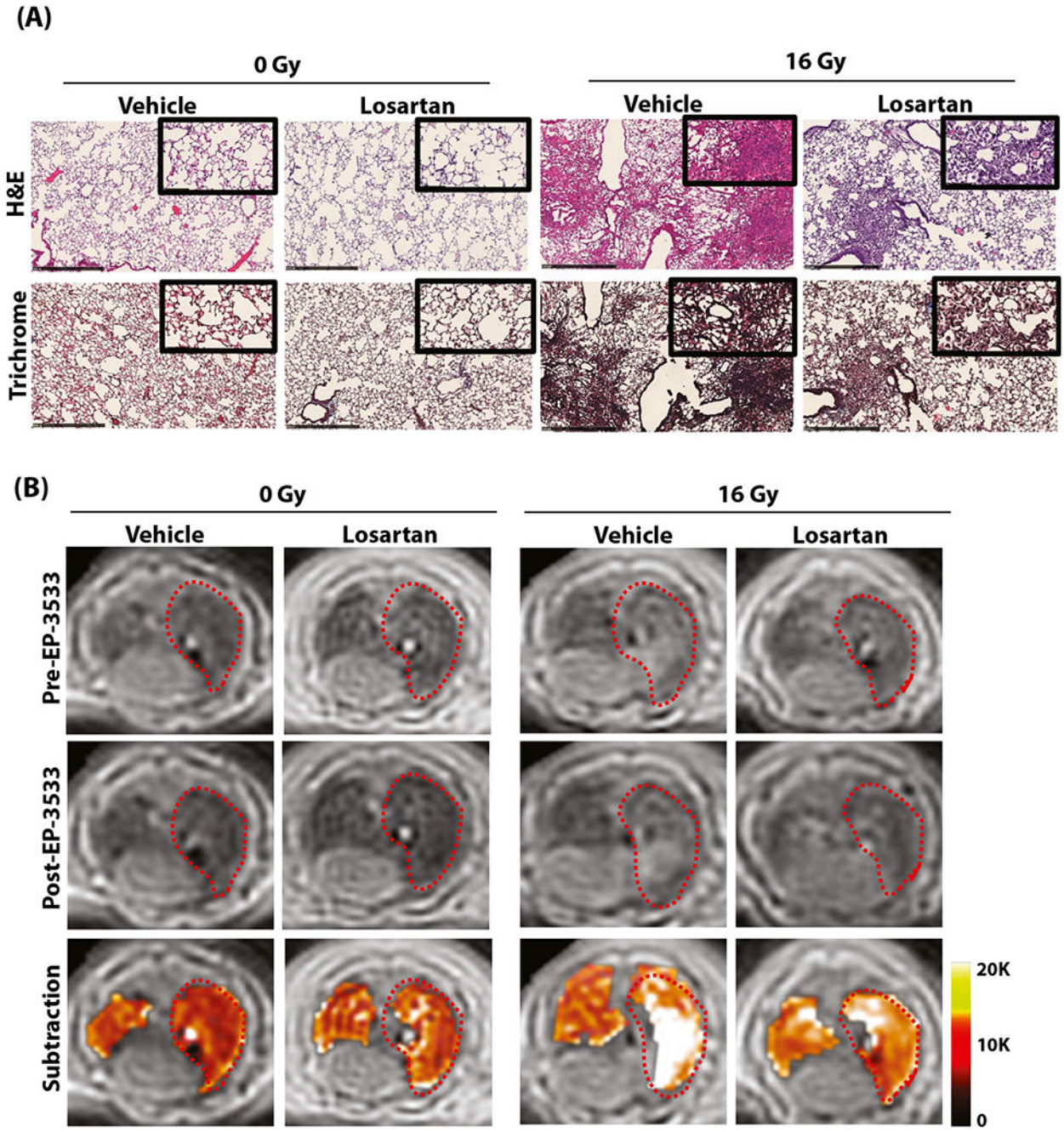

Fig. 3.

Mitigation of radiation-induced lung injury (RILI) with losartan in a murine model. (A) Representative hematoxylin and eosin (H&E; top) and trichrome (bottom) stains of the right lung show normal lung architecture in the 0-Gy groups, whereas the 16-Gy groups developed interstitial inflammation and alveolar thickening consistent with RILI, which is less severe in losartan-treated mice. (B) Representative axial magnetic resonance images before and after EP-3533 administration. Unirradiated (0-Gy) mice demonstrate low signal in both lungs, whereas irradiated mice demonstrate increased signal in the right lung

consistent with RILI. Images acquired 40 minutes after EP-3533 administration (middle) show increased lung signal in the irradiated mice compared with the preinjection images, although signal enhancement is diminished in mice treated with losartan. False color subtraction images (40 minutes following EP-3533 injection — preinjection) overlaid on preinjection ultra-short echo time images demonstrate increased signal enhancement in the irradiated lung and decreased signal enhancement in mice treated with losartan.

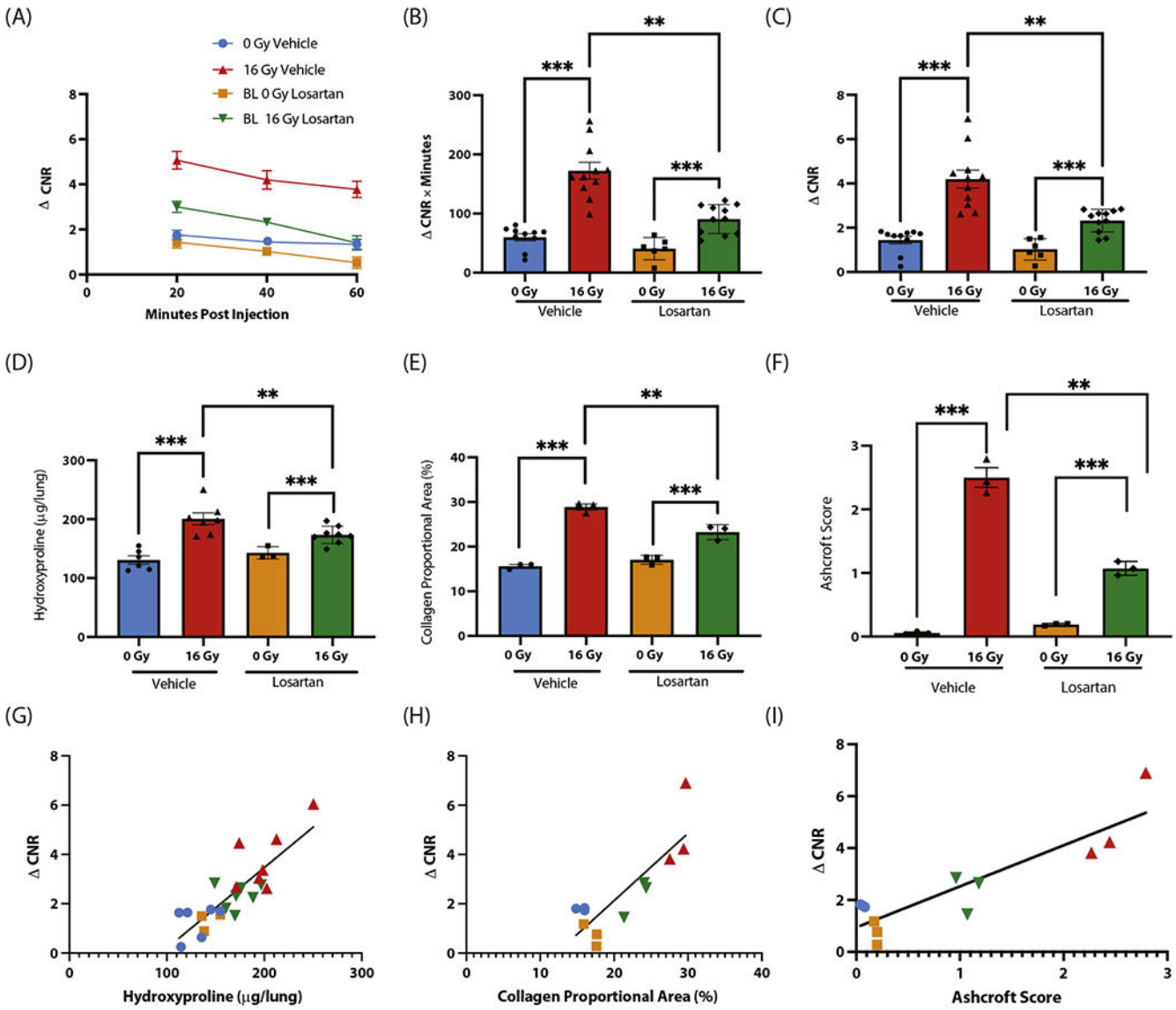

Fig. 4.

EP-3533 detects pharmacologic mitigation of radiation-induced lung injury with losartan in a murine model. (A) Change in contrast-to-noise ratio (ΔCNR) versus time curves demonstrate increased EP-3533 signal in the irradiated groups, although signal was reduced in the irradiated losartan group. (B, C) Area under the curve quantification (B) and ΔCNR at 40 minutes postinjection (C) revealed elevations in EP-3533 signal in the irradiated vehicle group, which was significantly reduced with losartan treatment. (D-F) Hydroxyproline (D), collagen proportional area (E), and Ashcroft score (F) each show significant increases with radiation, which are reduced in mice treated with losartan. (G-I) The associations between EP-3533 and hydroxyproline (G), collagen proportional area (H), and Ashcroft score (I) were assessed via Pearson correlation, and EP-3533 was significantly correlated with radiation-induced lung injury severity in each ($*P < .05$, $**P < .001$, $***P < .0001$).

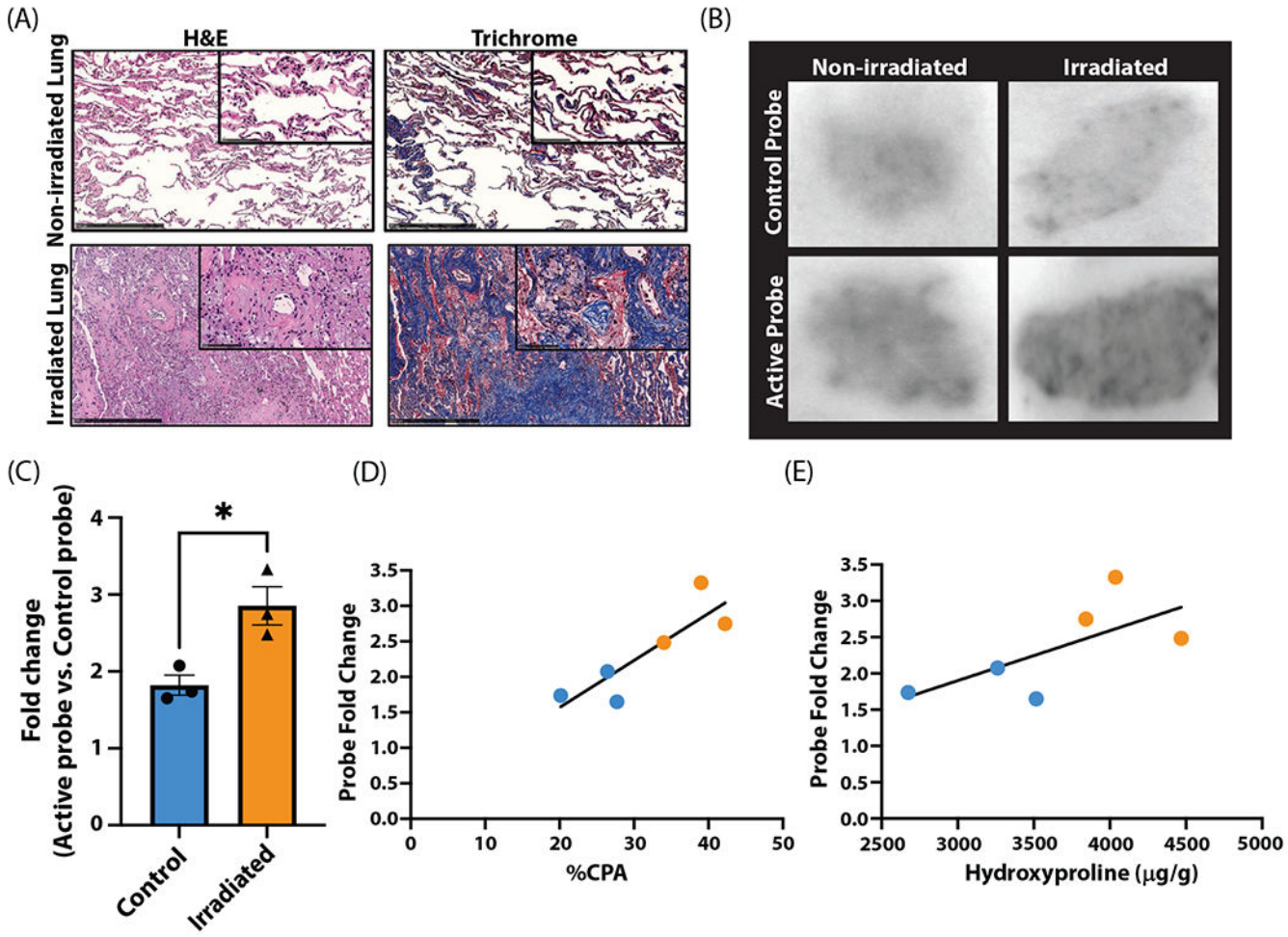

Fig. 5.

Quantification of ^{68}Ga-CBP8 in human tissue with radiation-induced lung injury. (A) Hematoxylin and eosin (H&E; left) and trichrome (right) stains of nonirradiated (top) and irradiated lung (bottom) with characteristic radiation-induced lung injury changes including cellular infiltration, alveolar wall thickening, and increased collagen deposition. (B) Autoradiography following incubation with ^{68}Ga-Ctrl shows similar uptake between irradiated and nonirradiated lung tissue (top). ^{68}Ga-CBP8 has increased uptake in irradiated versus nonirradiated lung tissue (bottom). (C-E) ^{68}Ga-CBP8 intensity normalized to ^{68}Ga-Ctrl signal intensity is significantly increased in irradiated tissue ($P = .021$; C) and is significantly correlated with collagen proportional area (CPA; $P = .026$; D) but not with hydroxyproline (E).

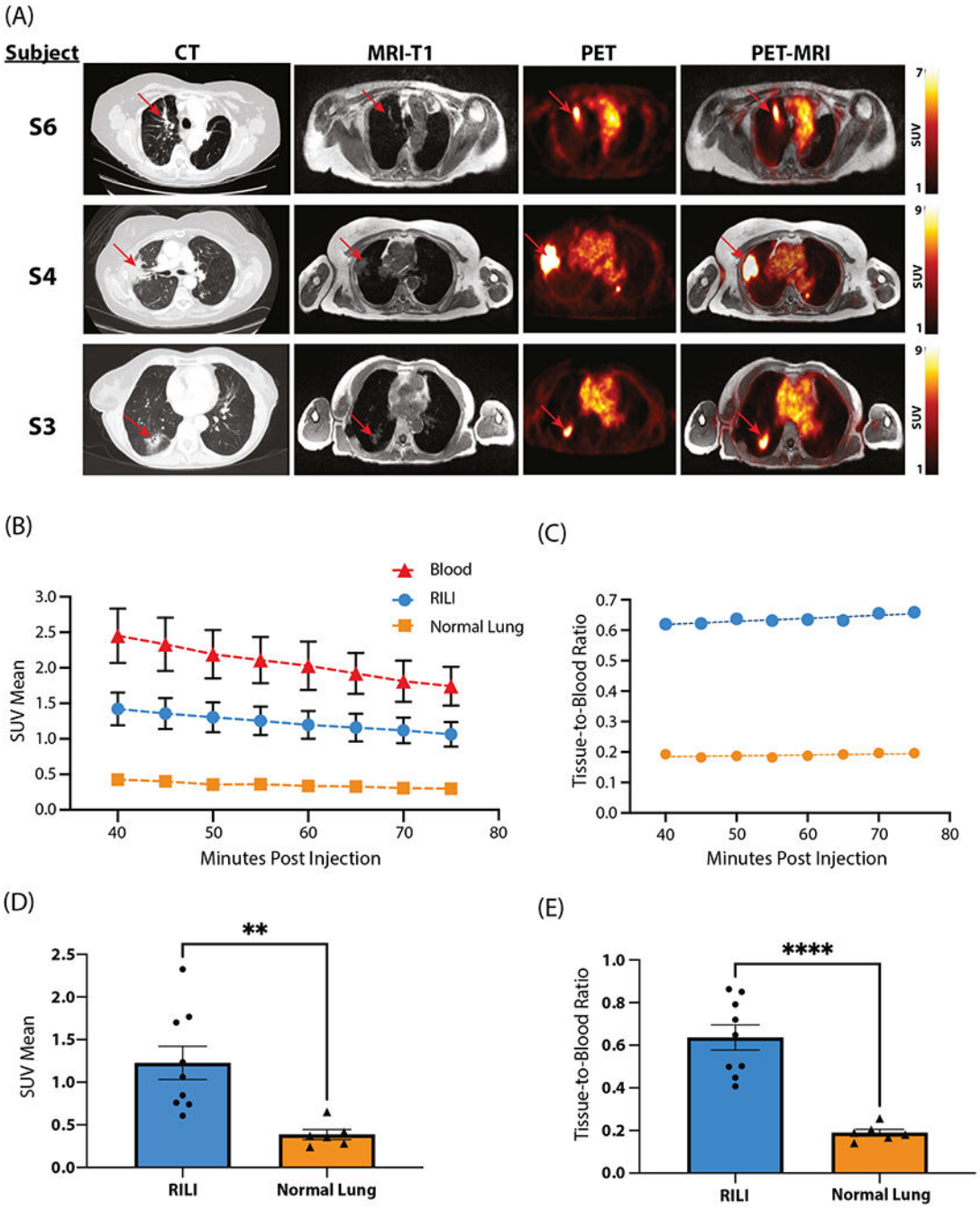

Fig. 6.

(A) Representative matching axial computed tomography (CT), magnetic resonance (MR), positron emission tomography (PET), and PET-MRI images of human participants with radiation-induced lung injury (RILI). Each row represents 1 individual. CT images (left) depict RILI in irradiated lung with characteristic consolidation and ground glass opacities. Red arrows indicate areas of RILI. Corresponding T1-weighted MR images obtained simultaneously with the PET study are shown in the second column. PET (third column) and fused PET-MRI images (fourth column) demonstrate elevated signal in areas of RILI

following the injection of ^{68}Ga-CBP8. (B-E) Quantitative analysis of ^{68}Ga-CBP8 PET images in individuals with RILI. (B) ^{68}Ga-CBP8 washout curves derived from dynamic PET images in areas of RILI, healthy lung, and blood pool. (C) Tissue-to-blood ratio for RILI and healthy lung. (D) Mean standardized uptake value (SUV) is significantly elevated in RILI versus in normal lung ($P = .005$). (E) Tissue-to-blood ratio is significantly elevated in RILI versus in normal lung ($P < .001$).